

Astrometry of Star Forming Region IRAS 05137+3919 in the far outer Galaxy

Mareki HONMA,^{1,2} Tomoya HIROTA,^{1,2} Yukitoshi KAN-YA,¹ Noriyuki KAWAGUCHI,^{1,2,3}
Hideyuki KOBAYASHI,^{1,4} Tomoharu KURAYAMA,⁵ Katsuhisa SATO³

¹Mizusawa VLBI Observatory, NAOJ, Mitaka, Tokyo 181-8588

²Graduate University for Advanced Studies, Mitaka, Tokyo 181-8588

³Mizusawa VLBI observatory, NAOJ, Mizusawa, Iwate 023-0861

⁴Department of Astronomy, University of Tokyo, Bunkyo, Tokyo 113-8654

⁵Graduate School of Science and Engineering, Kagoshima University, Kagoshima, Kagoshima 890-0065
mareki.honma@nao.ac.jp

(Received 2010 June 21; accepted 2010 October 12)

Abstract

We present the results of astrometric observations with VERA toward the H₂O maser sources in IRAS 05137+3919, which is thought to be located in the far outer Galaxy. We have derived the parallax of $\pi = 0.086 \pm 0.027$ mas, which corresponds to the source distance of $D = 11.6_{-2.8}^{+5.3}$ kpc. Although the parallax measurement is only 3- σ level and thus the distance uncertainty is considerably large, we can strongly constrain the minimum distance to this source, locating the source at the distance from the Sun greater than 8.3 kpc (or 16.7 kpc from the Galaxy's center) at 90% confidence level. Our results provide an astrometric confirmation that this source is located in the far outer Galaxy beyond 15 kpc from the Galaxy center, indicating that IRAS 05137+3919 is one of the most distant star-forming regions from the Galaxy center.

Key words: ISM: individual (IRAS 05137+3919) — Astrometry — VERA — techniques: interferometric

1. Introduction

Star-forming regions located in the far outer region of the Galaxy are interesting targets for astronomical studies in terms of both the Galactic structure and star formations. For examples, star-forming regions in the extremely outer Galaxy can be used to trace the extent of the Galaxy's stellar disk as well as the spiral structure in the outer regions. Also, star-forming regions in the far outer Galaxy provide unique laboratories to investigate how stars form in an extreme environment: in the far outer Galaxy, the metallicity is much lower than that in the Solar neighborhood (e.g., Smartt & Rolleston 1997; Rudolph et al. 2006), and hence the star-formation in the outer Galaxy at present could represent the star formation process in the early phase of galaxy evolutions, which are difficult to investigate through direct observations.

Currently several star-forming regions are expected to be located in the far outer region (here we define the far outer Galaxy as the region with the galacto-centric radius R_{GC} greater than 15 kpc). These star-forming regions have been mainly discovered based on extensive CO surveys toward the outer Galaxy (e.g., Wouterloot & Brand 1989; Digel et al. 1994), and the distances were estimated based on the kinematic distances obtained from observed radial velocities and assumed rotation curves. These surveys provided handful candidates of star-forming regions in the far outer regions, and in fact, some of them are intensively observed to study the star formation pro-

cess in an extreme environment (e.g., Ruffle et al. 2007; Kobayashi et al. 2008). However, since the distance estimates were based on the kinematic distances, there exist large distance uncertainties and hence the locations of such sources are yet to be confirmed with better accuracy. For instance, the star-forming region W3(OH), located in the Perseus arm, (though this is not the source in the far outer Galaxy) had a large discrepancy between the photometric distance and the kinematic distance, and accurate astrometries with phase-referencing VLBI (Xu et al. 2006; Hachisuka et al. 2006) revealed that the kinematic distance was an overestimation by a factor of two. The case for W3(OH) clearly demonstrated that the distance estimates based only on the kinematic distances are inadequate to conclude the locations of the star forming regions in the Galaxy. Fortunately, phase-referencing VLBI astrometry (such as using VERA and VLBA) are now powerful enough to determine accurate distances even beyond 5 kpc (e.g., Honma et al. 2007; Reid et al. 2009a), and hence astrometric measurements of star forming regions with VLBI will have great impact on the research of star-formation in the far outer Galaxy.

IRAS 05137+3919 is one of such star-forming regions which is thought to be located in the far outer Galaxy. The CO line was detected toward this source by Wouterloot & Brand (1989), catalogued as WB 621. The systemic velocity of CO was found to be -25.9 km s⁻¹, which provided a kinematic distance of 12 kpc. HCO⁺ line is associated with this source, with a systemic veloc-

ity of -26 km s^{-1} (Molinari et al. 2002). In HCO^+ line profile, a wing with a full width of 80 km s^{-1} was also detected, indicating molecular outflows from the forming star(s). Also associated with this source are infrared sources, dust continuum emission, compact HII regions, H_2CO absorption, OH, CH_3OH and H_2O masers (e.g., Brand et al. 1994; Molinari et al. 2002; 2008; Edris et al 2007; Araya et al. 2007; Sunada et al. 2007; Xu et al. 2008; Faustini 2009). Molinari et al.(2008) conducted a spectrum fitting to IRAS 05137+3919 from mm/sub-mm wave continuum taken with SIMBA at SEST and SCUBA at JCMT to infrared obtained with IRAS and MSX, and reported that the exciting source is likely to be an O8 ZAMS star with $L = 2.5 \times 10^5 L_\odot$. Thus, if the kinematic distance is correct, IRAS 05137+3919 is a massive star-forming region located at $R_{GC} \sim 20 \text{ kpc}$, which makes this source most interesting target to study the star formation in the extreme environment. However, since the source is located in the anti-Galactic center region, the kinematic distance, which is solely based on the radial velocity, would be highly uncertain. In order to measure the distance of IRAS 05137+3919 by means of trigonometric parallax, we have conducted the astrometry of H_2O maser and here report the results.

2. Observations

Observations of IRAS 05137+3919 were carried out with VERA using the dual-beam mode for the following eight epochs : DOY (day of year) 298 in 2007, DOY 5, 65, 147, 305 and 323 in 2008, and DOY 26 and 136 in 2009. However, the data for DOY 323 in 2008 was abandoned because of the bad weather conditions and high system temperatures, and hereafter we consider the remaining seven epochs for the astrometric analyses. During the 9-hour track of each epoch, we observed two target maser sources, IRAS 05137+3919 and 05274+3345, which are located closely in the sky plane (the results for the latter source will be presented elsewhere). In each epoch the on-source time for IRAS 05137+3919 was about 3 hours. The tracking position of $(\alpha_{J2000}, \delta_{J2000}) = (05\text{h}17\text{m}13.741\text{s}, \delta = +39\text{d}22'19.88'')$ was adopted, which is based on the observations by Migenes et al. (2000). The position reference source J0512+4041 $(\alpha_{J2000}, \delta_{J2000}) = (05\text{h}12\text{m}52.542843\text{s}, +40\text{d}41'43.62032'')$ was observed at the same time with the target maser source using the dual-beam system of VERA. The source separation between the position reference and the target maser is 1.56° . The position reference was fairly bright ($\sim 600 \text{ mJy}$) and always detected with sufficiently high S/N ratio throughout all the epochs. Furthermore, as a fringe finder, J0555+3948 ($\sim 2 \text{ Jy}$) was also observed and used to calibrate clock parameters for the correlation processing.

During these observations, the left-hand circular polarization were recorded with the VERA terminal at the data rate of 1 Gbps with 2-bit quantization. This provides total bandwidth of 256 MHz, which consists of 16 of 16-MHz IF sub-bands. The filtering of IF sub-bands were done by

using the VERA digital filter with one of 16-MHz bands assigned for the target maser source, and the remaining 15 of 16-MHz bands (240 MHz in total) assigned for the continuum sources such as the fringe finder and the position reference source. The frequency was set so that the H_2O maser line at a rest frequency of 22.235080 GHz came in the 16-MHz channel for the target maser source. Correlation processings were conducted with Mitaka FX correlator. The correlator accumulation period was 1 sec. For the continuum source, the spectral resolution was 64 points per 16-MHz sub-band, and for the maser source, 512 points per the 8 MHz (centered at the maser line in the 16-MHz channel), providing a frequency resolution of 15.625 kHz and a velocity resolution of 0.21 km s^{-1} , respectively.

3. Data Reductions

The data reduction processes were conducted with the software called VEDA (Vera Data Analyzer), which has been developed for the astrometric analyses of dual-beam observations with VERA. Since the delay model used in the correlation is not accurate enough for precise astrometry, before starting fringes searches, we have recalculated the delays of all the observed sources using the precise geodetic model and corrected for the differences of the two delay models. This precise recalculation of delay also included the most-updated earth-rotation parameters provided by IERS as well as tropospheric delays measured with GPS receivers at each station of VERA (see Honma et al. 2008a for troposphere calibration using GPS). Also, ionospheric delays were taken into account based on the Global Ionosphere Map (GIM), which was produced every 2 hour by University of Bern. In the following analyses, the visibilities were corrected for the delay difference between the crude delay used for the correlation and the precise recalculations for the astrometry.

At the beginning of fringe searches, fringes were searched for the fringe finder J0555+3948 and the clock offset and the clock rate offset were determined. Next the fringes were searched for the position reference J0512+4041, and the source image was obtained based on the self-calibration. The source structure was nearly point-like throughout the whole epochs, with a flux varying from 510 to 600 mJy. The synthesized beam was typically $1.6 \times 1.1 \text{ mas}$ with the position angle of 125° . Then, the residual phases found for the position reference were transferred to the maser source IRAS 05137+3919 to perform phase-referencing. When doing this, the instrumental phase difference between the dual-beam system was also calibrated based on the phase data obtained by the horn-on-dish method during the observations (Honma et al. 2008b). The phase-calibrated visibilities of the target maser source were integrated and Fourier-transformed to create dirty images of each maser channel, and then CLEANed to obtain the final maps from which the maser spots were identified. In the images of each epoch, maser spot positions were measured for brightness peaks brighter than 1.5 Jy .

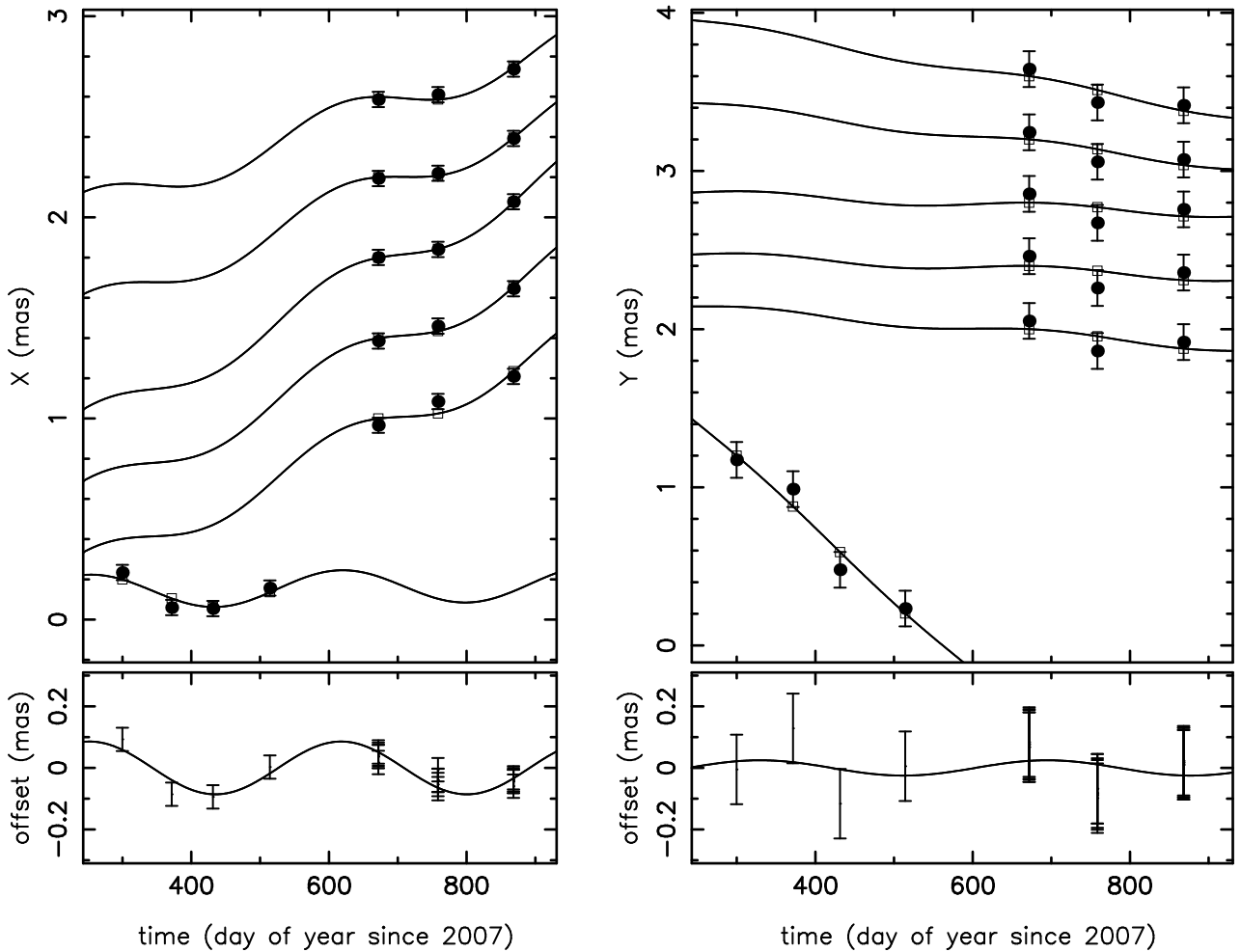


Fig. 1. Top: Motions of H₂O maser spots in IRAS 05137+3919 (filled circle with error bars). Left is for the right ascension and right for the declination. Note that for presentation purpose, constant offsets are added to observed positions. The curves are best-fit results based on the parallax of $\pi = 0.086$ mas (see text) and proper motions for individual spots, with open squares for the model value at the observed epochs. Bottom: The parallax components after removing the position offsets and proper motions. As seen in the parallax components, the data from the five spots from the same features are partially correlated, and this is why we have considered two different weights of these maser spots for the parallax determination.

To perform astrometry of the target maser spot, we used following criteria to identify maser spots in different epochs: 1) spots should be in the same velocity channel, 2) spot position difference should not exceed the proper motion threshold, which was set to be 10 mas yr^{-1} , 3) spots should be detected in continuous three epochs or more, and 4) spots should be compact (see below). Usually spot identifications are done based on the first two criteria (accordance of positions and velocities), but in the present paper we introduced additional two criteria 3) and 4) because we found the maser spots were highly variable from epoch to epoch: to avoid the misidentification of maser spots, we conservatively use maser spots that are persistent over continuous three epochs or more (criterion 3). In addition, to ensure the high precision, we selected compact maser spots based on the criterion 4. Concerning this criterion, we measured the spot size defined as the

area where the maser flux is larger than 30% of the peak flux, and if the spot size exceeds three times of the beam size, we identified it as “extended”, and removed from our analysis. We note that the required accuracy for parallax measurement of 10-kpc source is $\sim 10\text{-}\mu\text{as}$ level, which is nearly 1/100 of the beam size of VERA, and hence the maser spots with extended structures and their variations are not suitable for astrometry of distance sources.

Using above criteria, we identified six maser spots to be used for astrometric analyses in the present paper. Unfortunately however, due to the high variability of the maser spot, none of them were detectable throughout all the seven epochs. In fact, we found only one spot continuously detected for the first four epochs, and the remaining five spots were detected only for three epochs (see figure 1 and table 2). We note that the discontinuity of maser is not an artifact due to a bad epoch in the middle of moni-

toring period, but is a real feature due to the variation of maser intensities: as we have described in section 2, the epoch with a bad weather was already removed from the analyses in the present paper.

4. Astrometry

Since the maser spots are not persistent through the whole observing epochs and since the parallax is extremely small, we carefully carried out twofold fittings to obtain the parallax of IRAS 05137+3919. First we assumed the equal weight for all the six spots, and conducted astrometric fitting to the data with one common parallax π and proper motions for each spot ($\mu_{x,i}$, $\mu_{y,i}$). When performing the fitting, the error bars were assumed to be the same throughout all the maser spots and epochs: as is usual, it is not easy to estimate the astrometric accuracy of phase-referencing VLBI, and here we set the error bars so that the reduced χ^2 of the fit becomes unity. This process resulted in the error bar in the right ascension and the declination as $38 \mu\text{as}$ and $113 \mu\text{as}$, respectively. The larger error in the declination could be caused by the calibration error in the tropospheric zenith delay, although this source has relatively high declination. In this first fitting, we obtained the parallax $\pi_1 = 0.069 \pm 0.020$ mas.

However, as will be seen in figures 1 and 2 as well as table 2, the five spots (spot ID 1 to 5 in table 2) are associated with one maser feature (i.e., emitted from the same gas cloud), and thus the astrometric information obtained from the five spots may not be fully independent but partially correlated. In that case, using the equal weight for all the six spots could introduce some bias into the astrometric results. To avoid this, in the second fitting, we set the weight of the five maser spots to be 1/5 of the remaining one spot. This procedure can be regarded as the fitting by using two features (the feature with spot 1-5 and that with spot 6) with equal weight. In the second fitting, we obtained the parallax $\pi_2 = 0.103 \pm 0.021$ mas. This parallax is slightly larger than the first parallax π_1 . We note that the spot 6 tends to give a larger parallax than spots 1-5, and thus lowering the weight of spots 1-5 gives a larger parallax.

It is difficult to know how strongly astrometric data of spots 1-5 are correlated with each other. However we can safely assume that the reality lies between the two extremes, namely the two fittings described above. Hence, here we drive the final value of parallax for this source by taking the mean of the two fitting results, yielding the parallax of $\pi = 0.086 \pm 0.027$ mas. The error bar is obtained by combining in quadrature the scatter between π_1 and π_2 (which is ± 0.017 mas) and the individual parallax error of ± 0.021 mas. The results of parallax determination are summarized in table 1. The parallax corresponds to the source distance of $D = 11.6_{-2.8}^{+5.3}$ kpc. Although this is only $3 - \sigma$ level measurement of the parallax and thus is a marginal detection, this is one of the smallest parallax ever measured by means of trigonometric parallax.

Finally, using this parallax, proper motions of each spots were also obtained. In the proper motion deter-

Table 1. Summary of parallax determinations. Fits 1 & 2 are done based on the different weights, and the final value is obtained by taking the mean of the two. The error bar of the final parallax is determined by combining in quadrature the scatter of the individual parallaxes around the mean (± 0.017 mas) and the error bar of individual parallax (± 0.021 mas).

ID	note	π (mas)
fit 1	equal weight for six spots	0.069 ± 0.020
fit 2	equal weight for two features	0.103 ± 0.021
final	mean of the fit 1&2	0.086 ± 0.027

mination, a set of μ_x and μ_y were obtained for each maser spot by linear fitting after subtracting the effect of parallax. The results of proper motion determinations are summarized in table 2.

Figures 1 show the position variations of the six maser spots of IRAS 05137+3919 with respect to the position reference source J0512+4041. Here the constant position offsets are added for better presentation of the proper motion and parallactic motion of the spots. The top-left panel in figure 1 shows the time variations of the maser positions in the right ascension, and the top-right panel shows those in the declination. In figures 1, for comparison, we also plotted the fitting curves to the data, which consisted of the linear proper motions and parallax. From figures 1, one can clearly see that although the parallax detection is marginal, the fitting curves reproduce well the observed maser motions. This indicates that while the distance itself is still uncertain, the parallax for this source is fairly small. To illustrate this better, in the bottom of figures 1, we show the positional variations due to parallax after subtracting constant offsets and proper motions. In these figures, one can see that the parallax is considerably small, and the parallax derived here are consistent with data within the error bars. In fact, from the bottom panels of figures 1, one can see that the parallax cannot significantly exceed 0.1 mas. For instance, if the source is located at the distance of 5 kpc, which corresponds to a source in the outer arm (e.g., Honma et al 2007), it should have a parallax with an amplitude of 0.2 mas (and thus 0.4 mas in peak-to-peak), which is easily ruled out from the parallax components shown in figures 1. Thus, the results presented in this paper provide a strong lower limit of the distance to IRAS 05137+3919. Assuming Gaussian distribution of the probability distribution, the derived parallax of $\pi = 0.086 \pm 0.027$ mas provides a lower distance limit of $D_{\min} = 8.3$ kpc at 90% confidence level: this is evaluated by using $\text{erf}(x/\sqrt{2}\sigma) = 0.8$ (note that 0.8 instead of 0.9 for considering only one side of the Gaussian distribution corresponding to near distance rather than far distance) at $x = 1.28\sigma$ and hence $\pi_{\max} = 0.086 + 1.28 \times 0.027 = 0.121$ mas, corresponding to the minimum distance D_{\min} of 8.3 kpc.

Table 2. The best fit values of proper motions μ_X and μ_Y for the maser spots in IRAS 05137+3919. In the fit, the parallax of $\pi = 0.086 \pm 0.027$ mas is used. Note that positions X and Y are those at the epoch of 2007.0 with respect to the tracking center position of IRAS 05137+3919, which was taken to be (05h17m13.741s, +39d22'19.88") in J2000.

feature	spot ID	X (mas)	Y (mas)	V_{LSR} (km s $^{-1}$)	μ_X (mas yr $^{-1}$)	μ_Y (mas yr $^{-1}$)
1	1	37.556	29.882	-29.85	0.432 ± 0.102	-0.319 ± 0.304
	2	37.605	29.938	-29.64	0.524 ± 0.102	-0.213 ± 0.304
	3	37.676	30.019	-29.42	0.671 ± 0.102	-0.072 ± 0.304
	4	37.868	30.181	-29.21	0.634 ± 0.102	-0.079 ± 0.304
	5	38.012	30.314	-29.00	0.595 ± 0.102	-0.140 ± 0.304
2	6	-59.334	-70.050	-27.95	0.022 ± 0.090	-1.619 ± 0.269

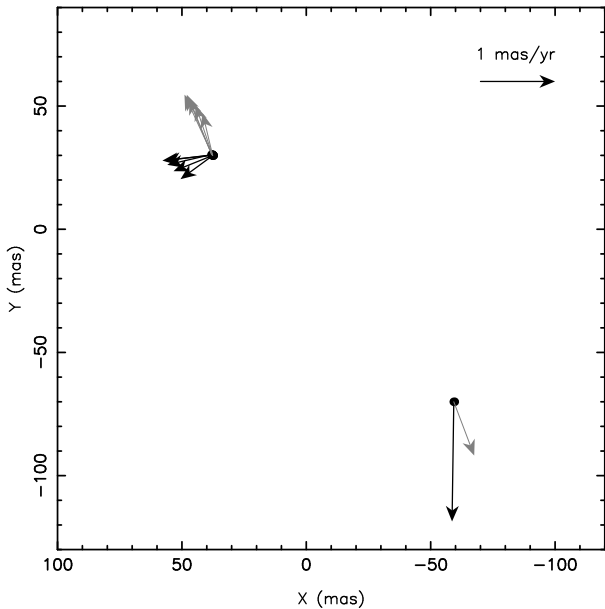


Fig. 2. Distributions of H $_2$ O maser spots in IRAS 05137+3919. Black vectors are proper motions obtained with respect to the position reference source. Grey vectors are internal maser motions that are obtained by correcting for estimated systematic motion of IRAS 05137+3919 (see text).

5. Discussions

5.1. Distance comparisons and location in the Galaxy

Previously the distance to IRAS 05137+3919 was estimated based on the kinematic distance. For instance, Wouterloot & Brand (1989) estimated the distance of $D = 12$ kpc assuming nearly flat rotation curve with $R_0 = 8.5$ kpc and $\Theta_0 = 220$ km s $^{-1}$, and a similar value was adopted in recent studies (e.g. Molinari et al. 2008, $D = 11.5$ kpc). On the other hand, our astrometric measurements provide a source distance of $D = 11.6^{+5.3}_{-2.8}$ kpc, and the minimum distance D_{min} of 8.3 kpc at 90%-confidence level. Although the uncertainty of our parallax distance is considerably large, there is no indication of systematic difference between the kinematic distances and the astrometric distance for this source, implying that the kinematic distances previously estimated were fairly reasonable. This

is in contrast to distance over-estimations using kinematic distance, found in such as W3(OH) in Perseus arm (e.g., Xu et al. 2006).

In the galacto-centric coordinate, the $1 - \sigma$ distance of $D = 11.6^{+5.3}_{-2.8}$ kpc from the Sun corresponds to $R_{\text{GC}} = 20.0^{+5.3}_{-2.8}$ kpc, and the minimum distance D_{min} of 8.3 kpc corresponds to the minimum Galacto-centric radius of 16.7 kpc (in both cases the IAU standard $R_0 = 8.5$ kpc is adopted). Therefore, the star-forming region IRAS 05137+3919 is most likely to be located beyond 15 kpc from the Galaxy and thus is in the far outer Galaxy. Hence, our results provide the first astrometric confirmation that there exist star-forming regions in the far outer regions of the Galaxy, demonstrating the existence of star formation activities in such region.

Currently the farthest spiral arm confirmed by astrometry is so-called Outer Arm. Recently VLBI astrometries of star forming regions in the Outer Arm have been carried out (e.g., Honma et al. 2007; Hachisuka et al. 2009), and the distance from the Sun to the Outer Arm in the direction of the Galactic anti-center is found to be 5 – 6 kpc (or $\sim 14 - 15$ kpc in Galacto-centric radius). We note that IRAS 05137+3919's location in the Galaxy is far beyond the Outer arm, and hence the location of this star-forming region in the Galaxy impose a question on how molecular clouds are formed in the far outer regions: whether there exists another (rather faint) spiral arm beyond the Outer arm, or there exist another mechanism to form a molecular cloud in such an extreme region.

5.2. Maser structure

Figure 2 shows the maser spot distributions in IRAS 05137+3919 with respect to the tracking center position. The maser spots are basically located in two maser features, one in the north-east (feature 1) and the other in the south-west (feature 2), with a separation of ~ 140 mas. In figure 2, maser proper motions with respect to the position reference source are also plotted (black arrows). Note that these proper motions include Galactic rotation of IRAS 05137+3919 itself as well as its systematic deviation from Galactic rotation (i.e., non-circular motion). To remove such effects and to see the internal motions of maser spots, we estimated the systematic motion as follows: first we average the maser motions in each feature (5 spots in the north-east feature and 1 spot in the south-west feature), which were found to be $(\bar{\mu}_X, \bar{\mu}_Y) = (0.571,$

-0.165) mas yr $^{-1}$ and $(0.022, -1.619)$ mas yr $^{-1}$, respectively. Then we obtained the systematic proper motion of IRAS 05137+3919 by taking the mean of the averaged motions of the two maser features, yielding $(\mu_{X,0}, \mu_{Y,0}) = (0.297, -0.892)$ mas yr $^{-1}$. The grey vectors in figure 2 are the internal maser motions obtained by subtracting the systematic proper motion. Interestingly, the directions of estimated internal motions are fairly close to the direction of elongation of the two maser features, and the internal maser motions shows that the separation of the two maser features are increasing. These results are consistent with a picture in which a bipolar outflow/jet from an exciting source (a proto-star in IRAS 05137+3919) forms two shock regions, where the maser emissions are observed.

The amplitude of the internal proper motions obtained above is about 0.78 mas yr $^{-1}$, corresponding to 43 km s $^{-1}$ using the distance of 11.6 kpc obtained in the present paper. This is significantly larger than the width of the radial velocity of H $_2$ O maser, which is only ~ 2 km s $^{-1}$. However, we note that the observations of HCO $^+$ by Molinari et al.(2002) reported a velocity wing with a width of ~ 80 km s $^{-1}$ (most-likely due to a large-scale outflow), which is fairly comparable with internal maser motions obtained here. Hence, the internal proper motion of 43 km s $^{-1}$ is not unlikely for this source. If the H $_2$ O maser in IRAS 05137+3919 indeed traces the outflow/jet motion, then the orientation of outflow/jet axis is nearly perpendicular to the line of sight. We note that the large-scale outflow traced with HCO $^+$ has a different orientation with the small-scale outflow traced with H $_2$ O maser emissions, because the high velocity wing of HCO $^+$ is seen in the radial velocity profile, indicating that the large scale outflow cannot be perpendicular to the line of sight, in contrast to the maser outflow. This may imply that the outflow orientation changes in different scales (due to, e.g., interaction with ambient matters and/or precession of outflow axis), or that there exist two different outflows from two independent exciting sources.

Note that the maser spot identification in the present studies was strictly done to ensure high precision in astrometry and hence some maser spots were removed from our analyses based on the four criteria described in section 3. In case that we loosen the criteria 3 and 4 in section 3 to include more spots, we found a few additional spots in the two features shown in figure 2, and also found one spot which is about 300 mas east of the two features shown in figure 2, which appears to be unassociated with the features in figure 2. Therefore, even if the selection criteria are modified, the basic maser structure presented in this chapter is not drastically changed.

5.3. Galactic Rotation in the far-outer Galaxy

Using the systematic motion of IRAS 05137+3919 obtained in section 5.2, we can constrain the Galactic rotation velocity in the far outer region. As we described above, by taking the mean of maser spot motions, we estimated the systematic motion of the source as $(\mu_{X,0}, \mu_{Y,0}) = (0.297, -0.892)$ mas yr $^{-1}$. By correcting for the standard solar motion of IAU 1985 with $(U_{\odot},$

$V_{\odot}, W_{\odot}) = (10.0, 15.4, 7.8)$ km s $^{-1}$ (Kerr & Lynden-Bell 1986), the motions of IRAS 05137+3919 with respect to the Local Standard of Rest are converted to be $(\mu_l, \mu_b) = (0.588, -0.130)$ mas yr $^{-1}$ in the Galactic coordinate. The proper motion along with the Galactic plane (μ_l) is considerably large, since the source is located toward the anti-center region ($l = 168.1^\circ$) and hence the proper motions of the source and the LSR should mostly cancel out. For instance, if we assume a flat rotation curve with $\Theta_0 = 220$ km s $^{-1}$, the expected relative proper motion of IRAS 05137+3919 with respect to the LSR along Galactic plane is $\mu_l = -0.071$ mas yr $^{-1}$ (at $D = 11.6$ kpc). Therefore, our results suggest that the Galactic rotation of IRAS 05137+3919 is smaller than that of a flat rotation curve by $\Delta v = 36$ km s $^{-1}$, which is obtained by using $D = 11.6$ kpc and the proper motion difference of $0.589 - (-0.071) = 0.660$ mas yr $^{-1}$ (note that this result is not significantly changed with different values of Θ_0).

Reid et al.(2009b) suggested that the massive star-forming region could rotate around the Galaxy slower than the Galactic rotation velocity by ~ 15 km s $^{-1}$. Our results for IRAS 05137+3919, rotation speed slower by 36 km s $^{-1}$, may be partly explained such a slow rotation of star forming regions. Also, the value of Δv is dependent of the source distance D , and if a smaller distance is adopted, the deviation from the flat rotation curve becomes small. For instance, if D_{\min} of 8.3 kpc is adopted, the difference from the flat rotation reduces to $\Delta v = 22$ km s $^{-1}$. However, even if this is the case, the discrepancy between the observed proper motion and the proper motion expected from the flat rotation curve still remains. This may suggest the Galactic rotation itself is slower in the far outer regions. However, since we have only one source in the far outer region and since the proper motion of this source could also be largely affected by modeled internal proper motions of maser spots (~ 43 km s $^{-1}$ as discussed in section 5.2), at this moment we cannot reach at a decisive conclusion. For further conclusion, we have to increase the number of sources in the far outer region for which accurate astrometry is done, which should be definitely one of the important future works of the VERA project.

One of the authors (MH) acknowledges financial support from grant-in-aid (No.21244019) from the Ministry of Education, Culture, Sports, Science and Technology (MEXT). Authors also would like to thank all the staffs at Mizusawa VLBI observatory and at Kagoshima University for supporting observations.

References

- Araya E., Hofner P., Goss W. M., Linz H., Kurtz S., Olim L., 2007, ApJS, 170, 152
- Brand, J., et al. 1994, A&AS, 103, 541
- Digel, S., de Geus, E., Thaddeus, P., 1994, ApJ, 422, 92
- Edris, K. A., Fuller, G. A., Cohen, R. J., 2007, A&A, 465, 865
- Faustini F., Molinari S., Testi L., Brand J., 2009, A&A, 503, 801
- Hachisuka K. et al., 2006, ApJ, 645, 337

- Hachisuka K. et al., 2009, ApJ, 696, 1981
Honma, M., et al. 2007, PASJ, 59, 889
Honma, M., et al. 2008a, PASJ, 60, 951
Honma, M., et al. 2008b, PASJ, 60, 935
Kerr F. J., Lynden-Bell D., 1986, MNRAS, 221, 1023
Kobayashi N., Yasui, C., Tokunaga, A., Saito, M., 2008, ApJ, 683, 178
Migenes, V., et al., 2000, ApJS, 123, 487
Molinari, S., Testi, L., Rodríguez, L., Zhang, Q., 2002, ApJ, 570, 758
Molinari, S., Pezzuto, S., Cesaroni, R., Brand, J., Faustini, F., Testi, L., 2008, A&A, 481, 345
Reid M. et al. , 2009a, ApJ, 705, 1548
Reid M. et al. , 2009b, ApJ, 700, 137
Rudolph A. L., Fich M., Bell G. R., Norsen T., Simpson J. P., Hass M. R., Erickson E. F., 2006, ApJS, 162, 346
Smartt S. J., Rolleston W. R., 1997, ApJ, 481, L47
Sunada K., Nakazato T., Ikeda N., Hongo S., Kitamura Y., Yang J., 2007, PASJ, 59, 1185
Wouterloot, J. G. A., Brand, J., 1989, A&AS, 80, 149
Xu Y., Reid M. J., Zheng X. W., Menten K. M., 2006, Sci, 311, 54
Xu Y., Hachisuka K., Pandian J., Menten K. M., Henkel C., 2008, A&A, 485, 729